Monthly Notices of the ROYAL ASTRONOMICAL SOCIETY

MNRAS **526,** 6145–6154 (2023) https://doi.org/10.1093/mnras/stad3006
Advance Access publication 2023 October 06

The 2021 mutual phenomena involving the Galilean satellites of Jupiter and the inner satellite Thebe

L. M. Catani [1,2★] M. Assafin [1,2★] B. E. Morgado,[1,2★] S. Santos-Filho,[1,2,3] F. Braga-Ribas,[4] R. Vieira-Martins,[2,5] J. Arcas-Silva,[2,5] A. C. Milone [6] I. J. Lima[6] and R. B. Botelho[6]

[1] *Universidade Federal do Rio de Janeiro (UFRJ), Ladeira do Pedro Antonio 43, Rio de Janeiro, RJ 20080-090, Brazil*
[2] *Laboratório Interinstitucional de e-Astronomia (LIneA), Rua Gal. José Cristino 77, Rio de Janeiro, RJ 20921-400, Brazil*
[3] *Centro de Educação a Distância do Estado do Rio de Janeiro (CEDERJ), Praça Cristiano Ottoni S/N – 6º andar, Rio de Janeiro, RJ 20221-250, Brazil*
[4] *Federal University of Technology – Paraná (PPGFA/UTFPR-Curitiba), Av. Sete de setembro 3165, Curitiba, PR 80230-901, Brazil*
[5] *Observatório Nacional/MCTI (ON), Rua General José Cristino 77, Rio de Janeiro, RJ 20921-400, Brazil*
[6] *Instituto Nacional de Pesquisas Espacias (INPE), Av. dos Astronautas, 1.758, São José dos Campos, SP 12227-010, Brazil*

Accepted 2023 September 28. Received 2023 September 28; in original form 2023 September 5

ABSTRACT

Astrometric studies and orbital modelling of planetary moons have contributed significantly to advancing our understanding of their orbital dynamics. These studies require precise positions measured over extended periods. In this paper, we present the results of the 2021 Brazilian Jovian mutual phenomena campaign. The data correspond to eight events between Galilean satellites, in addition to a rare eclipse of Thebe, an inner satellite, totalling nine events. A geometric model along with the DE440/JUP365 ephemerides was used to reproduce the events and simulate the light curves. A Monte Carlo method and chi-squared statistics were used to fit the simulated light curves to the observations. The reflectance model adopted for our simulations was the complete version of the Oren–Nayer model. The average uncertainty of the relative positions of the Galilean satellites was 5 mas (15 km) and for the inner Thebe satellite 32 mas (96 km). The seven mutual events (nine independent observations) here analysed represent an addition of 17 per cent events (10 per cent light curves) with respect to the 2021 international mutual phenomena campaign. Furthermore, our result of Thebe eclipse is only the second measurement published to date. Our results contribute to the ephemeris data base, being fundamental to improving satellite orbits and thus minimizing their uncertainties.

Key words: astrometry – eclipses – occultations – planets and satellites: individual: Io, Europa, Ganymede, Callisto, Thebe.

1 INTRODUCTION

The study of the orbital dynamics of satellite systems around giant planets is crucial for enhancing our understanding of the formation and evolution of the Solar system (Arlot & Stavinschi 2007). While the orbital evolution of these systems resembles that of objects in solar orbit, it occurs on a smaller time scale at a considerably faster rate. Consequently, investigating the physical aspects and dynamic evolution of planetary satellite systems becomes essential as it enables the examination of dynamic perturbations, including resonant and secular effects resulting from tidal dissipation (Lainey et al. 2009). Apart from shedding light on the system's dynamic evolution, these measurements are key in determining more accurate positions and updating their ephemerides.

In the Jovian system, there is a group of satellites located within the orbits of the Galilean moons. These small moons have a particular interest as they are believed to be the source of particles to Jupiter's ring system (Ockert-Bell et al. 1999). Studying the kinematics of these satellites helps us better understand the structure of Jupiter's rings and how they are maintained. However, due to the difficulty of observing these objects from ground-based observatories, the astrometry of these objects is particularly challenging (Veiga & Vieira Martins 1994).

The astrometric positions of Jupiter's main and inner satellites can be determined by observing mutual phenomena. These phenomena occur when one natural satellite eclipses or occults another from the perspective of an observer on Earth. Such events occur when the Earth and the Sun align with the common orbital plane of Jupiter's satellites. This particular alignment happens twice during each planet's orbit around the Sun. In the case of Jupiter, these alignments occur every six years, the last one being in 2021.

During mutual phenomena, we use photometry to measure object brightness variations over time. This technique precisely determines the relative positions between the satellites involved in the event (Emelyanov 2009; Arlot & Emelyanov 2019; Emelyanov et al. 2022). The astrometry with this method typically has an uncertainty of only about 5 mas, which is equivalent to about 15 km at Jupiter's distance (Emelyanov 2009; Dias-Oliveira et al. 2013; Arlot et al. 2014; Morgado et al. 2019a). For example, classical CCD astrometry exhibits uncertainties around 100 mas (∼300 km; Kiseleva et al. 2008), mutual approximations present uncertainties of the order of 10 mas (∼30 km; Morgado et al. 2016, 2019b), astrometric mea-

★ E-mail: lcatani@ov.ufrj.br (LMC); massaf@ov.ufrj.br (MA); bmorgado@ov.ufrj.br (BEM)

Table 1. Observational campaign details.

City/country	Station abbreviation MPC code	Telescopes Aperture	Longitude Latitude	Altitude	Observer	CCD	No. of positive detections
Itajubá/MG, Brazil	OPD	Boller & Chivens	45°34′57″W	1864 m	L. M. Catani	Andor-iXon^{EM}	6
	874	0.60 m	22°32′07″S	–	B. E. Morgado	–	–
	–	Perkin-Elmer	–	–	S. Santo-Filho	–	–
	–	1.60 m	–	–	J. Arcas-Silva	–	–
	–	–	–	–	A. R. Gomes-Junior	–	–
Curitiba/PR, Brazil	UTFPR	Meade-LXD55	49°20′23″W	935 m	F. Braga-Ribas	QHY174MGPS	2
	–	0.20 m	25°26′10″S	–	–	–	–
São José dos Campos/SP, Brazil	INPE	Celestron-C11	45°51′43″W	620 m	A. C. Milone	Watec 910HX	1
	–	0.28 m	23°12′32″S	–	R. B. Botelho	–	–
	–	–	–	–	I. J. Lima	–	–

Table 2. Observed events.

Date yy/mm/dd	Observer	Event (S_1xS_2)	Central (UTC)	Δt (min)	Flux drop
21/04/10	OPD	3ecl4	07:20	17.9	0.089
21/04/11	OPD	1ecl2	07:39	5.0	0.626
21/05/20	OPD	1ecl2	07:56	5.4	0.489
21/06/21	OPD	1ecl2	06:12	4.1	0.074
21/07/18	OPD	3ecl14	04:04	2.8	–
21/08/09	OPD	3occ2	06:17	29.1	0.157
21/08/09	UTFPR	3ecl2	03:37	67.5	0.465
21/08/09	UTFPR	3occ2	06:17	29.1	0.157
21/08/09	INPE	3ecl2	03:37	67.5	0.465

Note. Information about codes in the MPC and geographic locations of observation sites can be seen in the Table 1.

surements obtained via radio show minimum uncertainties around 0.5 mas (∼1.5 km; Brozović et al. 2020) and the technique of stellar occultations achieved an uncertainty of 0.8 mas (∼2.4 km; Morgado et al. 2019c, 2022). In addition, for the inner satellites, the average accuracy achieved through mutual phenomena for Thebe was around 45 mas (∼135 km; Saquet et al. 2016), and for Amalthea, it is 82 mas (∼246 km) as reported by Christou et al. (2010) and 47.8 mas (∼143 km) given by Morgado et al. (2019a).

This paper presents the results obtained from the analysis of the 2021 mutual phenomena of the Galilean satellites, including a rare eclipse involving the inner satellite Thebe (J14) of Jupiter. Mutual phenomena involving an inner satellite were first published by Christou et al. (2010) in 2019. Still, only one other event involving Thebe has been published so far by Saquet et al. (2016). Altogether, we analysed nine mutual phenomena involving Jupiter's satellites.

In Section 2, we provide the details of the observational campaign and the employed instrumentation. Section 3 presents the techniques used to mitigate the scattered brightness from Jupiter in the observed images with the *I* filter. The photometric reduction method of the observational data is addressed in Section 4. Sections 5, 6, and 7 delve into the modelling specifics, the process of fitting light curves, and parameter conversion. The results obtained and the conclusion are presented in Sections 8 and 9.

2 OBSERVATIONAL CAMPAIGN

In 2021, Jupiter entered its equinox. This provided an opportunity to observe mutual phenomena among the main Jovian satellites. The observations of the Brazilian mutual phenomena campaign in 2021 were carried out at the Pico dos Dias Observatory (OPD) and by observers in the south and south-east of Brazil. The predicted events were based on the ephemerides provided by the *Institut de Mécanique Céleste et de Calcul des Ephémérides* (IMCCE).[1,2]

We have gathered in Table 1 the information about the observational campaign: observation locations, data collection station abbreviations, MPC codes (when available), telescope apertures, geographic coordinates, altitude, observers, the sensor used, and the number of positive detections.

2.1 Selection of observed events

During the 2021 campaign, Jupiter had declination from −16° to −12°, which favoured observations in the Southern hemisphere.

A total of 192 mutual events were predicted for the Galilean satellites, visible for both hemispheres (Arlot & Emelyanov 2019). Of the total predicted events, only 47 would be observable from Brazil, and out of these, only 37 were visible from the observation sites. We selected 12 events among the Galilean satellites to be observed in our campaign. Additionally, we chose 6 events involving the inner satellites, specifically Thebe and Amalthea.

The observed events are listed in Table 2, which includes the dates of each event; the station; the type of event (ecl for eclipse and occ for occultations); and the satellites involved, 1 for Io, 2 for Europa, 3 for Ganymede, 4 for Callisto, and 14 for Thebe. In addition, the table also displays the expected central instant of each event, the duration, and the predicted magnitude drop. Note that, for events involving the inner satellites, the IMCCE does not provide predictions of flux drop for the events.

Of the eighteen selected events, we obtained nine light curves for analysis. The nine light curves were generated from seven different events, two of these seven events were observed by more than one observer, totalling nine light curves. The observed events are indicated in the third column of the Table 2. Of these events, we observe an eclipse between the inner satellite Thebe and Ganymede. The other events on the list were lost due to unfavourable weather conditions.

[1]Website: http://nsdb.imcce.fr/multisat/nsszph517he.htm
[2]Website: http://nsdb.imcce.fr/multisat/nsszph518he.htm

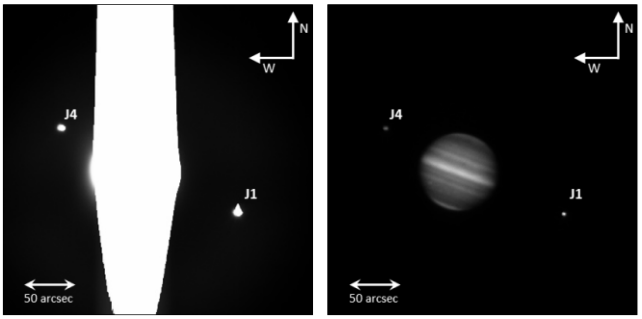

(a) I Filter of Johnson System (b) Narrow-band filter in 889 nm

Figure 1. Jupiter observed the two filters used during the campaign. The images were taken on 2021 July 5, with the 1.6 m Perkin-Elmer telescope, both with a one-second exposure time.

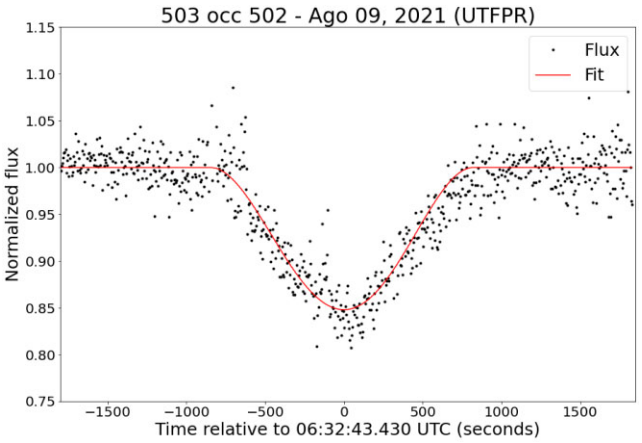

Figure 2. Light curve of an occultation between Ganymede (503) and Callisto (504) observed by UTFPR collaborators on 2021 August 9. The line represents the modelled flux of the event (see Section 5).

2.2 Instrumentation

The telescopes employed for observing the Galilean satellites had apertures ranging from 203 to 600 mm. For the observations of events involving the inner satellites, we specifically utilized the Perkin-Elmer 1.6 m telescope located at the OPD.

In observations involving only the Galilean satellites, we employed a narrow-band filter with a central wavelength of 889 nm and a bandwidth of 15 nm. This specific band falls within the methane absorption region of the electromagnetic spectrum. We deliberately chose this filter because, in this spectral range, Jupiter's albedo decreases to 0.05 as a result of absorption caused by the presence of methane in its upper atmosphere (Karkoschka 1998).

We show in Fig. 1b an image obtained using the Perkin-Elmer 1.6 m telescope at the OPD, providing an illustrative example of the methane filter effect. The planet and the satellites present about the same brightness due to the use of the narrow-band filter. This filter has been successfully used in the mutual phenomena campaigns of 2009 and 2014–2015 (Dias-Oliveira et al. 2013; Morgado et al. 2019a), as well as in the mutual approximation campaigns initiated in 2014 (Morgado et al. 2016, 2019b).

On the other hand, for observations of events involving the inner satellites, we used the *I* filter from the Johnson system, shown in Fig. 1a. We opted for this filter because it allows more light to pass through compared to the methane filter, favouring the capture of the faint brightness of the inner satellites and avoiding the complete saturation of the CCD, which would happen if no filter were used in the observation of Jupiter with a large telescope. In this context, it was necessary to apply additional processing to minimize the contribution of Jupiter's luminosity in the images, as explained in the next section.

3 TREATMENT OF THE IMAGES OBTAINED WITH AN *I* FILTER

In the images we observe using the *I* filter, we apply a technique to reduce part of the contamination of the scattered-light halo surrounding Jupiter over the inner satellites. This technique masks scattered light from Jupiter in the image. We construct a Jupiter model to subtract from the observed data. We construct the template using different sets of images from the same observation. In this context, when applying them to science images, it is necessary to take certain precautions to preserve the integrity of the scientific data. Some of these precautions include ensuring that the flux of the target object is not subtracted and ensuring that the telescope guiding is accurate enough to avoid significant variations in the observed field, as the effectiveness of this method relies on minimizing the movement of the contaminating source in the images.

The application of this technique is particularly useful for the inner satellites of Jupiter, which have a slightly faster orbital period, resulting in a significant displacement in the image field over short intervals of time. The result of this application can be seen sequentially in Fig. 3, where we have an original image with standard calibration (Fig. 3a), the template with the measured luminous contribution from the observations (Fig. 3b), and in Fig. 3c, the image after the applying this approach.

Note that this technique was applied after the standard bias and flat-field calibration, a procedure performed with the IRAF software (Butcher & Stevens 1981), the same used for the application of the technique detailed here.

4 PHOTOMETRIC REDUCTION

The astrometric study of mutual phenomena is conducted by analysing the light curves obtained from the observation of these events. Here, the light curves were generated with differential aperture photometry. This approach is particularly useful when you want to measure subtle variations in an object's luminous flux (magnitude) over time (Kjeldsen & Frandsen 1992). To build the light curves from the observations, we used the tasks of PRAIA (Package for the Reduction of Astronomical Images Automatically; Assafin 2011), which facilitated the analysis and processing of the data. The light curve is then normalized by a polynomial fit so that the flux ratio outside the flux drop gets equal to 1.0, and the flux drop can be adequately evaluated.

We present an example of light curves obtained with PRAIA in Fig. 2. The dots illustrate the normalized measurements of light flux, while the red line represents the modelled flux of the event, predicted by the DE440 + JUP365 ephemeris and adjusted based on the observations (see details in Section 5).

The light flux determination in each image was achieved through aperture photometry, integrating all the light flux within a specific area. This approach effectively eliminates atmospheric and sky background effects by referencing a calibration object. During an occultation, both satellites are measured together in the same aperture, and a third satellite is used as a calibrator. In the case of eclipses, the eclipsed satellite is measured alone in the aperture, and the eclipsing satellite (or any other) is used as a calibrator.

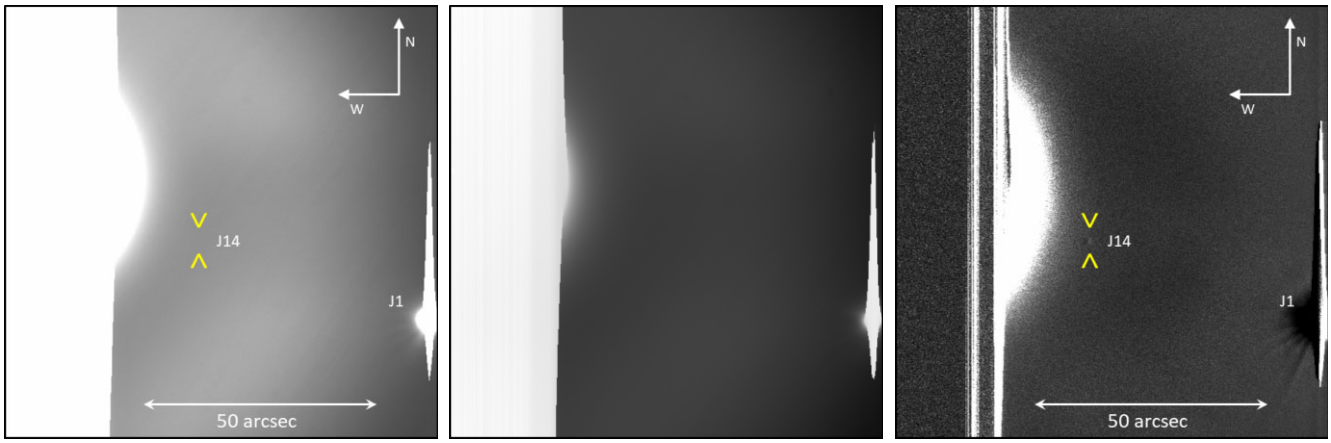

(a) Standard calibration (b) Template (c) After subtraction with template

Figure 3. Result obtained with the template technique. In (a) the image with standard treatment of *bias* and *flat-field*; in (b) the *template master* constructed for that set; and in (c) the image after applying the technique. The yellow arrow indicates Thebe's position in the image. This event was the eclipse between Ganymede (J3) and Thebe (J14) observed on 2021 July 18 by the Perkin-Elmer treaty applying 5 s of exposure using the *I* filter of the Johnson system.

Table 3. Information about photometric reduction.

Date yy/mm/dd	Observer	Event	Calib.	Aperture in pixels	σ of flux ratio
21/04/10	OPD	3ecl4	3	11	0.019
21/04/11	OPD	1ecl2	1	13	0.018
21/05/20	OPD	1ecl2	1	10	0.011
21/06/21	OPD	1ecl2	1	9	0.006
21/07/18	OPD	3ecl14	–	5	0.210
21/08/09	OPD	3occ2	–	6	0.017
21/08/09	UTFPR	3ecl2	3	2	0.043
21/08/09	UTFPR	3occ2	1	25	0.001
21/08/09	INPE	3ecl2	3	4	0.126

Note. Here, analogously to Table 2, we have: 1 = Io, 2 = Europa, 3 = Ganymede, 4 = Callisto, and 14 = Thebe.

In Table 3, we have gathered information regarding the photometric reduction of the nine light curves derived from our observations. In addition to the analogous information from Table 2, we display the calibration object used in the fourth column, the aperture size in pixels employed during the reduction in the fifth column, and the sigma values of the flux ratio in the last column. Note that for two events, we lack a calibration object. Therefore, the high frequency variations in flux for these events are a result of atmospheric effects that could not be eliminated.

5 METHOD FOR ANALYSING THE LIGHT CURVE AND OBTAINING ASTROMETRIC DATA

Here, we will discuss the method used to analyse light curves obtained from the observation and obtain astrometric data. Through the analysis of light curves from mutual phenomena, we can make precise measurements of the relative positions of the satellites involved in the event.

During the analysis of the curves, we seek to relate three parameters for the calculation of satellite positions. The parameters of interest in the analysis include the impact parameter (S_0), which is related to the smallest apparent angular distance between the satellites in the sky plane. In an occultation, this parameter refers to the minimum apparent distance between the satellites. In the case of an eclipse, it is related to the minimum apparent separation between the geometric centres of the eclipsed satellite and the shadow of the eclipsing satellite in the sky plane. Another parameter is the central instant (t_0), which refers to the exact instant when the smallest apparent distance between the satellites occurs. Additionally, the analysis also takes into account the apparent relative velocity (v_0) between the two satellites in the celestial plane.

These parameters are intrinsically linked to the dynamics and geometry of the satellites involved in the event. As a result, the value of each parameter has a direct relationship with the appearance of the light curves of the events. In this context, the analysis method used in this study involves the simulation of theoretical light curves for different values of each parameter. These theoretical curves are then compared to the light curves obtained from the observation, seeking the one that best fits the experimental data. This approach allows for the precise determination of parameter values and the obtaining of relative satellite positions.

5.1 Geometric model for the theoretical light curves

It is crucial to select an appropriate model to generate theoretical light curves, as the accuracy of simulated light curves depends on the chosen model for their construction. The geometric model we use to simulate theoretical light curves follows the principles described in Assafin et al. (2009), Dias-Oliveira et al. (2013), and Morgado et al. (2019a).

The adopted model simulates the light curve based on six parameters, which can be divided into two categories: physical parameters and dynamic parameters. The physical parameters of the model are the apparent sizes and shapes of each satellite and the albedo of the satellites in the case of occultations. The dynamic parameters are the ones we aim to obtain through the analysis, namely, the parameters of interest: S_0, t_0, and v_0.

The physical parameters, such as radius and shape, are naturally kept fixed during the modelling since they are determined with high precision from data collected by space probes. The albedos, on the other hand, are measured through auxiliary observations conducted before and after the events using the same instrumental configuration.

In some specific cases where it is not possible to obtain albedo measurements on the same night, previously determined albedo values are used.

On the other hand, unlike the physical parameters, the dynamic parameters are not fixed. By adopting different values for these parameters, it is possible to modify the appearance of simulated light curves. Based on this, a large number of theoretical light curves are generated using different sets of values for each parameter of interest. The curve that best matches the observed curve is selected. The fitting procedure follows the statistical method of chi-square minimization, as detailed in Section 6.

5.1.1 *Simulating eclipses and ocultations*

Now let us consider the differences between the simulation of eclipses and occultations. In general terms, the geometric model developed by Dias-Oliveira et al. (2013) and refined by Morgado et al. (2019a) constructs two-dimensional profiles based on the input parameters, simulating how the bodies are seen during these events by an observer on Earth.

To simulate an eclipse, the model constructs the disc of the eclipsed satellite and the shadow cast by the eclipsing satellite. A numerical model is used to reproduce the penumbra effect. In the case of occultations, instead of the shadow profile, the model reproduces the disks of the occulting and occulted satellites.

We used a reflectance model to simulate the reflection of light from the surface of the satellites with greater accuracy, as well as the effects of the solar phase. Following the steps of Morgado et al. (2019a), we employed the reflectance model proposed by Oren & Nayar (1994), which utilizes a general law for the reflection of non-homogeneous discs.

In both cases, eclipses and occultations, it is necessary to know the albedo of the satellites in the specific wavelength at which the observation is conducted. This is crucial to accurately represent the profile of each satellite exactly as they are observed.

In the case of occultations, it is necessary to calculate the albedo ratio since the measurement of the flux from both satellites is done using the same aperture. To do this, we measure the flux (F_1, F_2) of both satellites separately, using the same instrumental set-up. It is preferable to perform these measurements on the same night the event was observed.

The albedo ratio is then calculated using equation (1), which provides a relationship between the observed fluxes (F_1, F_2) with albedos (A_1, A_2) and the modelled fluxes (F_{S1}, F_{S2}).

$$\frac{F_1}{F_2} = \frac{A_1}{A_2} \cdot \frac{F_{s1}}{F_{s2}}. \tag{1}$$

Another important aspect is related to the physical parameters of the Sun, such as its radius, as well as using a model that considers limb darkening. The limb darkening effect was modelled according to the law of Hestroffer & Magnan (1998), with the parameters defined according to the spectral region of the observation.

Note that both limb darkening and reflectance are crucial elements for obtaining an accurate representation of the simulated light curves.

The final step in generating the light curves involves associating the modeled profiles with the actual observations. The code accomplishes this by simulating the flux F(t) of the satellites, integrating the modeled profile over the exposure times for each observation until the simulated light curve is obtained. Finally, the light curve is normalized outside of the event time window with respect to the flux of the eclipsed or occulted satellite, providing the simulated light curve.

6 FITTING LIGHT CURVES MODELS TO OBSERVATIONS CURVES

The fitting of the light curves involves comparing the observed light flux (f_i) with the modeled light flux (f_i') for each image (i) using the chi-squared method, as presented in equation (2).

$$\chi^2 = \sum_{i=1}^{N} \left(\frac{(f_i - f_i')}{\sigma} \right)^2. \tag{2}$$

Where σ was obtained by calculating the standard deviation of the observed light curve in the linear region outside the event.

The marginal uncertainties for a confidence level of 68 per cent (1σ) are determined from the parameters that result in χ^2 values less than $\chi^2_{\rm min} + 1$. For a good fit, it is expected that χ^2 is approximately equal to the degrees of freedom, which is defined as the difference between the number of data points (N) and the number of model parameters ($P = 3$).

Based on the adopted model, a large number of artificial light curves (about 900 for each event) are generated by varying the values of each dynamic parameter within a specific range. This range of values revolves around the predicted values for each event according to the DE440 + JUP365 ephemerides. Subsequently, corrections are applied to each light curve in order to find the parameters that minimize the chi-squared test. This procedure is performed using a PYTHON code developed by Morgado et al. (2019a).

7 CONVERTING PARAMETERS TO X AND Y

In our analysis, we obtain values for the impact parameter (S_0), central instant (t_0), and relative velocity (v_0), along with their corresponding offsets (ΔS_0, Δt_0, and Δv_0) with respect to the ephemerides. Using these results, we can calculate the apparent separation of the satellites in the sky plane following equation (3) introduced by Assafin et al. (2009). This approach serves as the theoretical basis for mutual phenomena and mutual approximations techniques (Morgado et al. 2016, 2019b; Santos-Filho et al. 2019).

$$S(t) = \sqrt{S_0^2 + v_0^2 (t - t_0)^2}. \tag{3}$$

On the other hand, we can express them in terms of right ascension ($X = \Delta\alpha \cdot \cos(\delta)$) and declination ($Y = \Delta\delta$) following Santos-Filho et al. (2019). Here, $\delta = (\delta_1 + \delta_2)/2$, $\Delta\alpha = (\alpha_1 - \alpha_2)$, and $\Delta\delta = (\delta_1 - \delta_2)$, where index 1 refers to the occulting/eclipsing satellite 1, and index 2 to the occulted/eclipsed satellite 2. Ephemeris offsets can be obtained using equation (4). Where θ represents the position angle of satellite 1 relative to satellite 2 in the plane of the sky (in the counterclockwise direction, with zero in the eastward direction), this angle is calculated from the topocentric positions of the satellites. Additionally, by convention, the relative velocity (v_0) is defined as negative/positive when it points towards an increase/decrease in θ at t_0.

$$\begin{aligned} \Delta X &= \Delta S_0 \cos(\theta) - \Delta t_0 \cdot v_0 \sin(\theta) \\ \Delta Y &= \Delta S_0 \sin(\theta) + \Delta t_0 \cdot v_0 \cos(\theta). \end{aligned} \tag{4}$$

The observed relative positions in X and Y can be calculated from the known relative distances obtained from the ephemerides and the values of (ΔX, ΔY). The uncertainties in (X, Y) are determined from the errors in t_0 and S_0.

8 RESULTS OF 2021 JUPITER'S MUTUAL PHENOMENA

The results of the mutual phenomena of Jupiter from the 2021 campaign were divided into two subsections. In the first one, we presented the analyses of the events that involved only the Galilean satellites. In the second one, we showed the results of the eclipse of the inner satellite, Thebe.

8.1 Galilean satellite events

Here we present the results of the events that involved only the Galilean satellites. The individual results for each parameter of interest can be seen in Table 4. Table 5 shows the topocentric results for the positions X and Y.

Table 4 presents, in the first three columns, the date, event type, and observer, as defined in Tables 1 and 2. In the following columns, we show the results for the impact parameters (S_0), central instant (t_0), and relative velocity (v_0). Additionally, the deviations (O–C) between the observations and the JPL DE440 + JUP365 ephemerides are provided. The deviations are represented by ΔS_0, Δt_0, and Δv_0. In the last two columns, we display the number (N) of used images and the normalized χ^2. At the bottom of the table, the means and standard deviations (S. D.) are presented.

Table 5, with the first three rows analogous to Table 4, also presents the results in terms of topocentric distances X and Y between the pair of satellites involved in the event (occulting/eclipsing satellite minus occulted/eclipsed satellite), as well as the uncertainties (σX, σY), the ephemeris offsets (ΔX, ΔY) and the number of points used to fit the curves (N). The means and standard deviations for the parameters are provided at the bottom of the table, similarly to Table 4.

Fig. 4 displays the plots with curve fitting for each event involving the Galilean satellites observed during the 2021 campaign. In the top panel of each plot, the uniform line represents the model, and the nonuniform curve shows the normalized flux. In the lower panel, the resulting residual from the model's fit to the observations.

The albedo ratio between Ganymede and Callisto could not be determined for the occultation that occurred on August 9th. This was because the satellites involved in the occultation were not sufficiently separated to measure the individual flux from both in the images obtained. Therefore, to avoid a significant loss of precision, the same albedo ratio values published by Morgado et al. (2019a) were used, where the albedo ratio between Ganymede and Callisto was 1.61.

According to Table 4, the average errors achieved in our analyses were as follows: for the impact parameter, the average error was 4.7 mas; for the central instant, we obtained an average error of about 4.6 mas; and regarding the relative velocity, the average error was 0.2 mas s^{-1}.

As for the ephemeris offsets, which represent the differences between the observed and predicted values, we obtained the following results: for the impact parameter, the mean offset was −5.6 mas with a standard deviation of 5.1 mas; for the central instant, the mean offset was +0.8 mas with a standard deviation of 2.21 mas; and for the relative velocity, the mean offset was + 0.01 mas s^{-1} with a standard deviation of 0.05 mas s^{-1}. All these values can be found in Table 4. The accuracy of our analyses was 2.4 mas.

The error values are consistent with the dispersion of the ephemeris offsets, with no mean offsets greater than 1 sigma (1σ). Therefore, we can conclude that the JPL DE440 + JUP365 ephemerides are in good agreement with the observations from the 2021 campaign of mutual phenomena of the Galilean satellites, at the level of 5 mas.

8.2 Eclipse of Thebe

In the observations of the mutual phenomena in 2021, we were able to record, using the 1.6 m telescope at the OPD, a rare eclipse between the satellites Ganymede and the inner satellite Thebe, which occurred in the early morning of 2021 July 18. Performing astrometry of Thebe through mutual phenomena is a challenging task due to the proximity of the satellite to Jupiter (with a semimajor axis equivalent to 3.17 Jupiter radii), which often causes obstruction due to the scattered brightness of the planet.

To overcome the mentioned observational problems, the coronography technique is commonly applied. This technique has shown positive results for performing astrometry of the inner satellites, as it allows the separation of the satellite from Jupiter's scattered light (Christou et al. 2010; Saquet et al. 2016; Robert et al. 2017; Morgado et al. 2019a).

However, we opted for a different approach and applied a technique of subtracting Jupiter's scattered light from the observational data by constructing a model of the planet's scattered flux (see Section 5). This approach was innovative in the analysis of mutual phenomena, and the results were very promising, making it feasible and opening new avenues for the analysis of mutual phenomena involving Jupiter's inner satellites.

Note that the first observation of a mutual phenomenon involving the inner satellite Thebe was reported by Saquet et al. (2016), who published the results of an eclipse of Thebe by Callisto observed during the 2014/2015 campaign. Thanks to our observational efforts and analysis approach, we were able to provide the second observation of a mutual phenomenon involving Thebe.

The photometry of this data set was also performed using the PRAIA package (Assafin 2011). However, for this event, during the reduction process, we manually defined the photometric aperture to achieve the best signal-to-noise ratio. It is worth noting that for these data, we do not have a photometric calibrator available (see Table 3), and therefore, systematic variations in the light curve of this event are related to changes in the night's weather conditions.

The simulations and light curve fitting of the eclipse of Thebe were conducted following the approach described in Section 5. However, due to Thebe's irregular shape (triaxial diameter of 116 × 98 × 84 km), in our simulations, we considered the satellite as a sphere with a radius of 49.3 km, with an uncertainty of 4 km (Thomas et al. 1998). This choice does not affect the accuracy of the measurements, as the relative velocity of the event involving Thebe is about 9.5 mas s^{-1} (∼28 km s^{-1}), and with a temporal resolution of 5 s in our measurements, coupled with the resolution of our observations (∼140 km), the real shape of the satellite becomes indistinguishable from the approximate shape.

The results obtained from the observation of the eclipse of Thebe are compiled in Table 6. The parameters listed in the first column are: the central instant t_0; the impact parameter S_0; the relative velocity v_0; the standard deviation σ (O–C); the number N of data points used in the fitting; and the value of the minimum chi-squared per degree of freedom found with the curve fitting. In the second column, we provide the values predicted by the JPL DE440 + JUP365 ephemerides; in the third column, we display the results obtained from the curve fitting; and finally, in the fourth column, we present the offsets between the observations and the ephemerides (O–C). As before, the JPL DE440 + JUP365 ephemerides were used in this analysis.

Fig. 5 displays the light curve fitting of Thebe. Similar to plots of Fig. 4, the upper panel shows the curve representing the observation, and the uniform line represents the fitted model. In the lower panel, the residual of the fit.

Table 4. Results of the parameters of interest obtained for the Galileans.

Date (y/m/d)	Event S_1xS_2	Obs.	S_0 (mas)	Error (S_0) (mas)	t_0 UTC (h:m:s)	Error (t_0) (s)	v_0 (mas s^{-1})	Error (v_0) (mas s^{-1})	ΔS_0 (mas s^{-1})	Δt_0 (mas)	Δv_0 (mas)	N	χ^2
21/04/10	3ecl4	OPD	1331.8	3.57	07:30:29.33	1.06	2.31	0.10	− 3.48	− 2.72	+0.03	242	0.538
21/04/11	1ecl2	OPD	295.9	1.25	07:41:37.81	0.44	7.36	0.22	− 0.96	− 1.36	− 0.10	297	0.811
21/05/20	1ecl2	OPD	466.9	1.54	07:58:40.32	0.45	6.31	0.50	+1.89	− 0.15	− 0.10	169	0.700
21/06/21	1ecl2	OPD	908.5	10.8	06:14:38.47	0.92	5.28	0.79	− 10.81	+2.10	+0.06	86	0.609
21/08/09	3ecl2	UTFPR	414.3	3.68	04:13:38.90	6.45	0.61	0.05	− 11.60	+2.09	+0.01	717	0.323
21/08/09	3ecl2	INPE	413.2	9.17	04:13:43.27	18.11	0.62	0.05	− 12.80	+4.98	− 0.02	1645	0.521
21/08/09	3occ2	OPD	958.3	3.17	06:32:43.79	3.18	1.21	0.07	− 4.10	+0.44	− 0.02	172	0.859
21/08/09	3occ2	UTFPR	958.3	4.46	06:32:44.25	3.47	1.23	0.08	− 3.04	+1.29	− 0.01	250	0.741
Mean	–	–	–	4.70	–	4.61	–	0.23	− 5.61	+0.83	+0.01	–	–
S. D.	–	–	–	3.24	–	2.66	–	0.25	5.07	2.21	0.05	–	–

Table 5. Results in X and Y for events among Galileans.

Date (y/m/d)	Event S_1xS_2	Obs.	X (mas)	Y (mas)	σX (mas)	σY (mas)	ΔX (mas)	ΔY (mas)	N
21/04/10	3ecl4	OPD	+444.3	− 1255.5	3.47	2.57	+1.42	− 4.19	242
21/04/11	1ecl2	OPD	− 97.6	+280.4	3.47	0.21	+0.96	− 1.36	297
21/05/20	1ecl2	OPD	+163.6	− 437.3	2.17	2.46	+0.80	+1.72	169
21/06/21	1ecl2	OPD	+326.8	− 848.2	0.58	11.83	− 5.88	− 9.32	86
21/08/09	3ecl2	UTFPR	− 182.6	+397.7	2.07	4.99	− 6.70	− 9.70	717
21/08/09	3ecl2	INPE	− 185.6	+397.7	6.30	12.92	− 9.82	− 9.60	1645
21/08/09	3occ2	OPD	− 402.8	+876.6	2.26	4.51	− 2.12	− 3.54	172
21/08/09	3occ2	UTFPR	− 402.7	+875.2	2.02	5.87	− 2.46	− 2.22	250
Mean	–	–	–	–	2.79	5.67	− 2.97	− 4.77	–
S. D.	–	–	–	–	1.57	4.21	3.86	4.03	–

The uncertainty achieved for the impact parameter, as indicated in Table 6, reached 2.4 mas. For the relative velocity, the error was 1.1 mas s^{-1}, and for the central instant, it was 6.7 s mas between the observed and predicted values. The offsets were +4.2 mas for the impact parameter, 1.5 mas s^{-1} for the relative velocity, and 11.6 mas for the central instant.

Table 7 displays the results concerning the right ascension (α) and declination (δ) directions for the positions (X, Y). The information contained in Table 7 is analogous to that of Table 5. It is noteworthy that the errors σX and σY in the topocentric positions were, respectively, 39 mas (∼117 km) and 51 mas (∼153 km).

9 CONCLUSION

In this study, we present the results of nine light curves obtained from the observation of seven different mutual events of Jupiter in 2021. The observed events involved the Galilean satellites, and one particular event included the inner satellite Thebe. The observations were conducted at the OPD and by collaborators in the south and south-east regions of Brazil. Telescopes with apertures ranging from 0.20 to 1.60 m were used for the observations.

The analysis method we employed involves applying simulation routines and curve fitting techniques described in Sections 5 and 6, as published in Morgado et al. (2019a). During our fitting process, we encountered average offset values that are below 1 sigma (1σ). The minimum average precision obtained for events involving only the Galilean satellites was 2.8 mas (∼8.4 km), as shown in Table 5. For the Thebe eclipse, we achieved a minimum precision of 38.8 mas (∼116.7 km). Based on these results, it can be concluded that our modelling aligns well with the observational data, demonstrating a strong agreement between the model predictions and actual observations.

The results derived from our analyses, combined with the extensive set of observations of this system, are significant for quantifying variations in the orbits and velocities of the satellites. These measurements can be utilized to enhance the uncertainties associated with the orbits of the Galilean satellites and Jupiter's inner satellite,– Thebe.

More precise ephemerides of Jupiter's satellite orbits, especially the Galilean satellites, are crucial for the planning of space missions aimed at this system, as well as the optimization of ongoing missions. In this context, the Europa Clipper mission,[3] scheduled to launch in 2024, and the JUpiter ICy moons Explorer (JUICE) probe,[4] launched in 2023 April with an expected arrival at the Jovian system in 2031, stand out. Both probes will derive precise space astrometry with flies by all Galilean moons, except Io (Fayolle et al. 2023). This further enhances the importance of our study, as three out of the five independent events here analysed involve Io.

Furthermore, periodic measurements of the orbits of the Galilean satellites enable the study of low-intensity effects that are less explored, such as resonant effects and tidal dissipation (Lainey et al. 2009).

Through the observation and data processing techniques mentioned in Sections 2 and 3, we were able to observe the second mutual phenomenon involving the inner satellite Thebe. This was first reported by Saquet et al. (2016) based on observations from the 2014–2015 campaign. This approach is particularly intriguing as

[3]Website: https://europa.nasa.gov/
[4]Website: https://www.esa.int/Science_Exploration/Space_Science/Juice

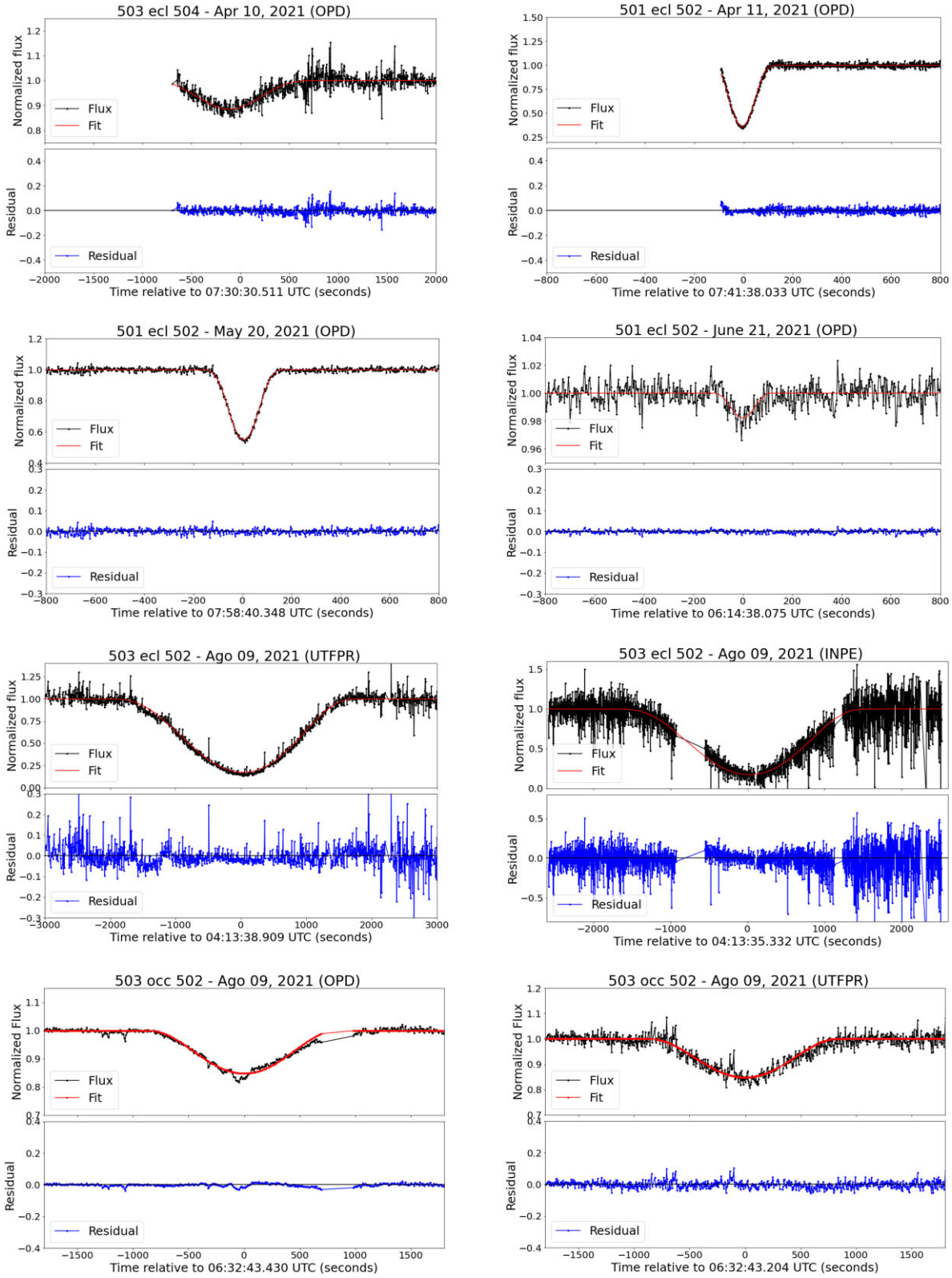

Figure 4. Fitting of the eight light curves of events between the Galilean satellites. The graph title indicates the satellites, event, date, and observer. The upper panel of each figure displays the fitting of the light curves, and the lower panel shows the residuals of the fitting.

Table 6. Results of the eclipse of Thebe by Ganymede in 2021.

Parameters	Ephemeris	Observed (error)	(O–C)
t_0 (h:m:s)	04:05:18.271	04:05:19.491 (6.883 s)	+11.64 mas
S_0 (mas)	816.50	820.67 (2.435)	+4.164
v_0 (mas s^{-1})	8.044	9.547 (1.097)	+1.503
σ (O–C)	–	0.279	–
N	–	43.00	–
χ^2	–	0.731	–

Note. The time is given in UTC.

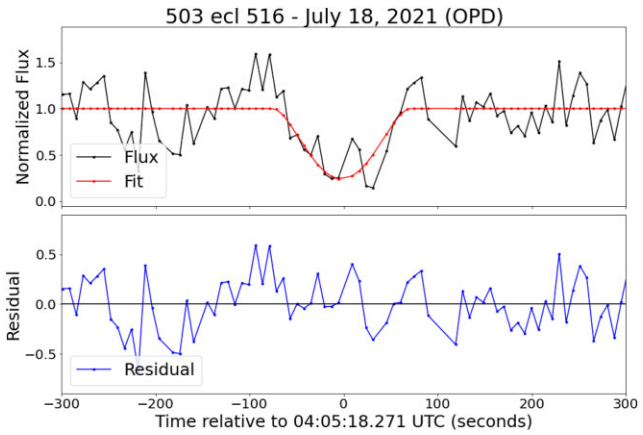

Figure 5. Light curve fit of an eclipse between Ganymede (503) and Thebe (514) observed on 1.6 m telescope on OPD in 2021 July 18.

Table 7. Results in X e Y for the eclipse of Thebe by Ganymede on 2021 July 18.

X (mas)	Y (mas)	σX (mas)	σY (mas)	ΔX (mas)	ΔY (mas)	N
+301.74	−763.26	38.86	51.06	−9.17	+8.28	43

it paves the way for future studies of mutual phenomena involving Jupiter's inner satellites or even the reevaluation of observations from previous campaigns.

In the context of this work, we encourage the continuous observation of mutual phenomena occurring among the moon of giant planets. The next mutual phenomena of Jupiter is expected to take place between 2026 and 2027, and an observational campaign for these events will be organized for that occasion. Additionally, it's worth emphasizing the significance of observing the 2024–2026 campaign for the mutual phenomena of Saturn. After the conclusion of the Cassini mission, the Saturnian system requires new astrometric measurements to maintain the precision of its satellite ephemerides. Predictions for the upcoming mutual phenomena of Jupiter and Saturn can be consulted on the IMCCE website (Arlot & Emelyanov 2019).[5]

ACKNOWLEDGEMENTS

We express our sincere gratitude to the group of observers who collaborated to make this work possible. We also extend our thanks to the team at the Pico dos Dias Observatory for their support and technical assistance during the observations, which took place amidst the crisis triggered by the COVID-19 pandemic. M.A. thanks CNPq grants 427700/2018-3, 310683/2017-3, and 473002/2013-2. B.E.M. thanks CNPq grant 150612/2020-6. F.B.R. acknowledges CNPq grant number 314772/2020-0. R.V.M thanks grant CNPq 307368/2021-1. I.J.L acknowledges São Paulo Research Foundation (FAPESP) for financial support under grant 2015/24383-7 and 2013/26258-4 This study was based in part on observations made at the Pico dos Dias Observatory, managed by the Laboratório Nacional de Astrofísica (LNA), Itajubá-MG, Brazil. We also received observations from collaborators in Brazil's southern and southeastern regions. This study was funded by the Coordenação de Aperfeiçoamento de Pessoal de Nível Superior – Brasil (CAPES), Finance Code 001.

DATA AVAILABILITY

The data that support the results and plots in this paper and other findings of this study are available at the Natural Satellites Data Base (NSDB)[6] (Arlot & Emelyanov 2009), or directly available from the corresponding author upon reasonable request.

REFERENCES

Arlot J.-E. et al., 2014, A&A, 572, A120
Arlot J.-E., Emelyanov N., 2019, Planet. Space Sci., 169, 70
Arlot J. E, Emelyanov N. V., 2009, A&A, 503, 631
Arlot J.-E., Stavinschi M., 2007, in Demircan O., Selam S. O., Albayrak B., eds, ASP Conf. Ser. Vol. 370, Solar and Stellar Physics Through Eclipses. Astron. Soc. Pac., San Francisco, p. 58
Assafin M., 2011, Praia - platform for reduction of astronomical images automatically. In: Gaia Follow-Up Network for the Solar System Objects: Gaia FUN-SSO WorkshopProceedings. p. 85
Assafin M., Vieira-Martins R., Braga-Ribas F., Camargo J., da Silva Neto D., Andrei A. H., 2009, AJ, 137, 4046
Brozović M. et al., 2020, AJ, 159, 149
Butcher H., Stevens R., 1981, Kitt Peak Natl. Obs. Newsl., 16, 6
Christou A., Lewis F., Roche P., Hidas M., Brown T., 2010, A&A, 522, A6
Dias-Oliveira A. et al., 2013, MNRAS, 432, 225
Emelyanov N. et al., 2022, MNRAS, 516, 3685
Emelyanov N., 2009, MNRAS, 394, 1037
Fayolle M., Magnanini A., Lainey V., Dirkx D., Zannoni M., Tortora P., 2023, A&A, 677, A42
Hestroffer D., Magnan C., 1998, A&A, 333, 338
Karkoschka E., 1998, Icarus, 133, 134
Kiseleva T., Kiselev A., Kalinichenko O., Vasilyeva N., Khovricheva M., 2008, Sol. Syst. Res., 42, 414
Kjeldsen H., Frandsen S., 1992, PASP, 104, 413
Lainey V., Arlot J.-E., Karatekin Ö., Van Hoolst T., 2009, Nature, 459, 957
Morgado B. et al., 2019a, Planet. Space Sci., 179, 104736
Morgado B. et al., 2019b, MNRAS, 482, 5190
Morgado B. et al., 2019c, A&A, 626, L4
Morgado B. et al., 2022, AJ, 163, 240
Morgado B., Assafin M., Vieira-Martins R., Camargo J., Dias-Oliveira A., Gomes-Júnior A., 2016, MNRAS, 460, 4086
Ockert-Bell M. E., Burns J. A., Daubar I. J., Thomas P. C., Veverka J., Belton M., Klaasen K. P., 1999, Icarus, 138, 188

[5]Website: http://nsdb.imcce.fr/multisat/nssephme.htm

[6]Website: http://nsdb.imcce.fr/obsphe/obsphe-en/

Oren M., Nayar S. K., 1994, in Proceedings of the 21st Annual Conference on Computer Graphics and Interactive Techniques techniques. ACM, New York, p. 239
Robert V., Saquet E., Colas F., Arlot J.-E., 2017, MNRAS, 467, 694
Santos-Filho S., Assafin M., Morgado B., Vieira-Martins R., Camargo J., Gomes-Júnior A., Benedetti-Rossi G., 2019, MNRAS, 490, 3464
Saquet E., Emelyanov N., Colas F., Arlot J.-E., Robert V., Christophe B., Dechambre O., 2016, A&A, 591, A42
Thomas P. et al., 1998, Icarus, 135, 360
Veiga C., Vieira Martins R., 1994, A&AS, 107, 551

This paper has been typeset from a TEX/LATEX file prepared by the author.